Shock Waves (1994) 4:15–23

Shock Waves

Unstructured adaptive remeshing finite element method for dusty shock flow

S. Sivier[1], E. Loth[1], J. Baum[2], R. Löhner[3]

[1] Department of Aeronautical and Astronautical Engineering, University of Illinois at Urbana-Champaign, Urbana, IL 61801, USA
[2] Science Applications International Corporation, McLean, VA 22102, USA
[3] CMEE, School of Engineering and Applied Science, The George Washington University, Washington, D.C. 20052, USA

Received November 17, 1992; accepted June 2, 1993

Abstract. The passage of planar shocks in a dusty gas was investigated to note effects due to particle loading and initial shock Mach number. Two-phase flow equations have been added to a conservative, monotonic flow solver to allow study of compressible particle and droplet flows, which are of importance for shock propagation in two-phase flows and spray propulsion systems. The formulation developed herein employed a conservative Eulerian treatment for the gas and particle phases. The computations were performed using the finite element method-flux corrected transport (FEM-FCT) scheme, which has shown excellent predictive capability of various compressible flows which include both strong and weak shocks. The flux limiting technique was modified to provide monotonic particle velocity fields to increase the scheme's computational stability. Adaptive unstructured methodology based on adapting to high gradients of both the fluid and particle densities was used in conjunction with the conservative shock-capturing scheme to adequately resolve strong flowfield gradients. The shock attenuation of this scheme was then compared with previous experimental and numerical results and was found to yield robust predictions. Various interphase coupling terms were also considered to note their effect on the shock attenuation.

Key words: Adaptive unstructured grid, Dust, Finite element, Particles

1. Introduction

Two-phase compressible flow phenomena present an important field of study for engineering systems which include: solid rocket motors, shock induced dust lofting, detonations, and sprays in high speed jet engines. Experimental and computational studies are needed to provide detailed analysis of such flow fields and to allow increased understanding necessary for improved engineering design.

Correspondence to: E. Loth, 104 S. Wright Street, Room 306, MC-236, Department of Aeronautical and Astronautical Engineering

When solving the compressible two-phase equations, the continuum gas dynamics are usually best represented by an Eulerian description, that is, the gas characteristics are calculated at fixed points within the flow. However, as the particles may be relatively sparse in the flowfield, the particles can be modeled by either an Eulerian description (in the same manner as the gas flow) or a Lagrangian description (where individual particle groups are monitored and tracked in the flow). Both descriptions have been used extensively (Crowe 1982), but for particles present throughout a large extent of the computational domain, the Eulerian description is typically a more efficient approach. In the present study, this Eulerian approach is coupled with an unstructured finite element method to take advantage of the beneficial aspects of an adaptive grid strategy. Adaptive grids can provide high resolution of the particle gradients as well as the flow gradients, e.g. shocks and slip layers.

1.1. Previous studies

Sommerfeld (1985) performed experiments to study the attenuation of a shock as it propagated into a gas-particle mixture. A vertical shock tube was used to provide a planar shock interaction with a homogeneous air-particle mixture. Glass spheres with an average diameter of 27 μm were used for the particles. The shocks were generated in pure air and propagated upward into the dusty flow. A number of tests were run at different initial shock speeds M_0 and particle loadings η (the ratio of particle mass to gas mass in a given volume of mixture). A one-dimensional numerical scheme was used to examine the dusty shock attenuation were also conducted using the random-choice method by adding the particle phase equations in an Eulerian manner.

Igra and Ben-Dor (1980) conducted a one-dimensional numerical study of the relaxation zone behind a normal shock in a dusty gas. The particle phase was added in an Eulerian fashion and various representations of the drag coefficient, C_D, and the Nusselt number, Nu, were examined, including effects of compressibility. Only minor changes were noted in the relaxation lengths and no comparison with experiment was made. Additional one-dimensional nu-

merical studies based on Sommerfeld's experimental data were conducted by Olim et al. (1987), using an Eulerian two-phase formulation in conjunction with a finite difference FCT (flux corrected transport) method. In this scheme, the limiting was applied before the dissipative interphase coupling terms were added. The study was used to show that the attenuation of the shock wave takes the form of an exponential decay curve and to examine the variations that result from particle loading and diameter changes. The choice of FCT showed marked improvement over Sommerfeld's random-choice method for predicting an M_0 of 1.25 with a particle loading of 0.63.

Crowe (1982) presented a review of numerical models for two-phase flow. Both Eulerian and Lagrangian methods were discussed and compared for structured finite difference calculations. Eulerian methods allow particle diffusion to be incorporated into the model, whereas Lagrangian methods typically require less memory overhead when particles of different sizes are considered and when particles rebound off of boundary surfaces.

1.2. Current study

The objective of the present study is to incorporate Eulerian two-phase flow methodology into a state-of-the-art finite element, two-dimensional compressible flow solver. This new computational technique will allow enhanced simulations of dusty shock flows over complex shapes by taking advantage of the mesh adaptive, shock-capturing ability of FEM-FCT (finite element method flux corrected transport). This approach is evaluated with experimental results of one-dimensional wave attenuation in a dusty gas (Sommerfeld 1985; Olim et al. 1987). In addition, the empirical interphase coupling terms for energy and momentum were studied to examine their effects on solution sensitivity and robustness.

In modeling the flowfield, the following usual assumptions were incorporated: the particles do not significantly contribute to the gas pressure, the particle volume fraction is negligible, the particles are spherical, inert, of uniform size and temperature, and are also dilute, i.e., particle-particle interactions do not account for a significant portion of the forces on the particles. Since the particle density, ρ_p, is more than three orders of magnitude larger than the surrounding gas density, ρ, the added mass effect is neglected. Since the quiescent terminal velocities of the particles are much less than typical shock accelerating gas velocities, gravitational effects are also neglected. Finally, since the gas velocity gradients through which the particles will be convected have scales much larger than the particle diameter (except at the shock), Basset history terms are also neglected. Thus, the only forces acting on the particles (pressure and viscosity) can be described based on a single coefficient of drag. As for the energy coupling, the effects of radiation can be considered negligible since phase temperature differences are not excessive; therefore, heat transfer can be expressed simply in convective terms based on a constant Prandtl number.

2. Numerical method

2.1. Gas equations

The following is a brief summary of the numerical method and the implementation of the gas-particle equations used in this study. For more detail of FEM-FCT applied to the Euler equations (single-phase), see Löhner et al. (1987). The two-phase flow equations are written in conservation form as

$$\frac{\partial \mathbf{U}}{\partial t} + \frac{\partial \mathbf{F}_j}{\partial x_j} = \mathbf{S} \tag{1}$$

where the summation convention is used for the four conservation equations of mass, momentum and energy:

$$\mathbf{U} = \begin{bmatrix} \rho \\ \rho u_i \\ \rho e \end{bmatrix}, \quad \mathbf{F}_j = \begin{bmatrix} \rho u_j \\ \rho u_i u_j + p\delta_{ij} \\ u_j(\rho_e + p) \end{bmatrix}, \quad \mathbf{S} = \begin{bmatrix} 0 \\ -D_i \\ -Q - u_{pi} D_i \end{bmatrix} \tag{2}$$

where D_i is the component of particle drag force per unit volume of the gas in the direction x_i of a Cartesian coordinate system, and Q is the heat transferred from the gas to the particles. The state equations are

$$p = (\gamma - 1)\rho\left(e - \frac{1}{2}u_j u_j\right), \quad T = \left(e - \frac{1}{2}u_j u_j\right) C_V \tag{3}$$

where ρ, p, e, T, k, γ, and C_V are density, pressure, specific total energy, temperature, thermal conductivity of the fluid, ratio of specific heats, and specific heat at constant volume, respectively, and u_i is the component of the fluid velocity in the direction x_i. Thus, the fluid is assumed to be compressible with viscous effects confined to the interaction with the particles (although artificial viscosity is present in the numerical scheme).

The higher order solution chosen for FEM-FCT is obtained via a two step form of the Taylor-Galerkin scheme of Donea (1984), which has been used for the computation of inviscid and viscous flows for the Cartesian (Löhner et al. 1989; Baum et al. 1990) and axisymmetric coordinate systems (Löhner et al. 1989; Loth et al. 1990a; 1990b). The Taylor-Galerkin scheme is used to increase the order of the approximation of the time derivative and produce a second order scheme. The spatial discretization is implemented with the usual Galerkin weighted residual method. The scheme involves two steps (Löhner et al. 1985), which together progress the solution from time t^n to time $t^{n+1} = t^n + \Delta t$. Quantities with integer timestep values (t^n and t^{n+1}) are located at nodes and have piecewise linear shape functions, denoted by N_j for a given node j. At the half timesteps, ($t^{n+1/2}$) quantities are centered at the elements and have piecewise constant shape functions for a given element, e. Solution with the consistent mass matrix is achieved by iterating with the lumped mass matrix. For the explicit two step Taylor-Galerkin scheme, a Courant type stability condition (Löhner et al. 1985) is applied to each element to obtain a local time step, Δt_e; from this a maximum CFL of 0.25 is used for the global timestep.

To formulate the FCT approach, the low order scheme must be monotonic and is simply obtained by inexpensively adding 'mass-diffusion' to the high order scheme (Löhner et al. 1987). The low order solution and the high order solution can then be combined to yield monotonic conditions for the conserved quantities near discontinuities and a second order solution in the rest of the domain, through the FEM-FCT formulation. The six steps of FEM-FCT are defined as:

1) Compute the high order element contribution (HEC) from the high order scheme.
2) Compute the low order element contribution (LEC) from the low order, monotonic scheme (which is based on diffusing the high-order scheme).
3) Define the antidiffusive element contribution (AEC), where AEC = HEC − LEC.
4) Compute the updated low order solution: $\mathbf{U}_l^{n+1}$.
5) Limit the AEC such that $\mathbf{U}^{n+1}$ found in step 6 below is free of extrema not present in $\mathbf{U}^n$ or $\mathbf{U}_l^{n+1}$, i.e. $\mathrm{AEC}^c = C_{el} \cdot \mathrm{AEC}$, where $0 \leq C_{el} \leq 1$.
6) Apply this limited AEC^c, i.e. $\mathbf{U}^{n+1} = \mathbf{U}^n + \mathrm{AEC}^c$.

Crucial to this procedure is the limiting method used to calculate C_{el} in step 5. To maintain strict conservation, this limiting is carried out on the four unknowns (ρ, ρu, ρv, and ρe) at the element level (Löhner et al. 1984). Zalesak (1979) showed that the original limiting method of Boris and Book (1976) needs to be modified for multi-dimensional flow problems. For a system of PDE's such as that in (1), it is typical for one global C_{el} to be chosen in some manner from the individual C_{el}'s of the four unknown fluxes. For the current study, a limiter based on the minimum of the C_{el}'s for ρ and ρe was found to be sufficient to guarantee monotonicity in the gas unknowns while minimizing the diffusion caused by the low order element contribution.

Adaptive H-refinement was employed to optimize the distribution of grid points by refining areas with high gradients of density and coarsening areas of low gradients of density. This allows efficient use of memory and computational time. In general, such refinement may reduce storage and CPU requirements by 10–100 times in advection-dominated flows as compared to an overall fine grid (Löhner et al. 1987). As in previous studies, a local 'error indicator' was used to determine if a given element needed to be refined, coarsened, or left alone based on the H_2-seminorm.

2.2. *Particle description*

For the two dimensional case, five particle equations (Olim et al. 1987) were added to solve for the five particle unknowns: spatial density σ, x-particle velocity u_{p1}, y-particle velocity u_{p2}, particle energy e_p, and number density n. The two densities are defined as:

$$\sigma = \frac{(\text{mass of particles})}{(\text{unit volume of gas})}$$

$$\text{and } n = \frac{(\text{number of particles})}{(\text{unit volume of gas})}.$$

The two different density definitions are employed to allow for a variable particle diameter, such as occurs in combustion or evaporation. The mass loading of the particles is then defined as $\eta = \sigma/\rho$. The equations then become:

$$\frac{\partial \mathbf{U}_p}{\partial t} + \frac{\partial \mathbf{F}_{pj}}{\partial x_j} = \mathbf{S}_p \tag{4}$$

where:

$$\mathbf{U}_p = \begin{bmatrix} \sigma \\ \sigma u_{pi} \\ \sigma e_p \\ n \end{bmatrix}, \quad \mathbf{F}_{pj} = \begin{bmatrix} \sigma u_{pj} \\ \sigma u_{pi} u_{pj} \\ u_{pj} \sigma e_p \\ n u_{pj} \end{bmatrix},$$
$$\mathbf{S}_p = \begin{bmatrix} O \\ D_i \\ Q + u_{pi} D_i \\ O \end{bmatrix}. \tag{5}$$

The two-step second-order Taylor-Galerkin algorithm discussed above is used to solve the homogeneous parts of the gas and particle equations. The gas/particle coupling terms (drag and energy transfer) are then calculated separately and added to yield the particle HEC, as is done for the gas phase equations. From this, the low order contribution may be calculated. The HEC and LEC were combined through flux limiting similar to,but separate from the gas equations to yield a monotonic flowfield. Note that this is not the same technique used by Olim et al. (1987) where the dissipative terms were added after the flux limiting, and which incorporated individual limiters for each of the conservation equations. By employing a more conservative flux limiter and applying it after the interphase coupling terms are added (as is done herein), the addition of the LEC may be reduced resulting in a scheme of potentially higher order accuracy.

Determining a proper limiter for the particle equations occupied a significant portion of the methodology development. Using a limiter based on the particle spatial density σ was found to leave a non-monotonic solution in u_{pi} at the interface between regions with gas only and regions with gas and particles. A limiter based on the conservative flux σu_{pi} gave similar results. These oscillations in u_{pi}, when combined with several levels of mesh refinement at the particle density interface, even led to unstable solutions. This was probably due to the fact that the interphase coupling drag is based on the difference in velocity between the gas and the particle, as opposed to a difference in momentum. The oscillations arose because the σu_{pi} discontinuity at the interface extends over fewer cells than the σ discontinuity. Therefore, large peaks will form in u_{pi} at the interface, even though σ and σu_{pi} are monotonic (see Fig. 1).

It was found that basing the limiter on the non-conservative variable u_{pi} removed most of the oscillations in u_{pi}. This was accomplished by transforming the contributions to non-conservative form in order to find the amount of LEC required to prevent no new undershoots or overshoots of u_{pi} in terms of a C_{el}, then returning the contributions to conservative form and proceeding as in the gas equations. Small oscillations remained due to a final scatter of element values to nodes of the conserved quantities, but these had little effect on the solution. Similar to the gas density ρ, a scheme for refining and coarsening the mesh was applied to σ in order to provide an accurate description of any particle

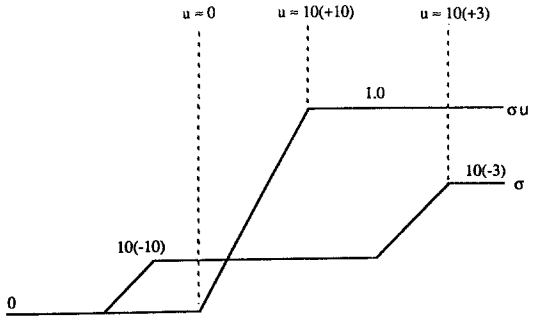

Fig. 1. Schematic of non-monotonic behavior in velocity

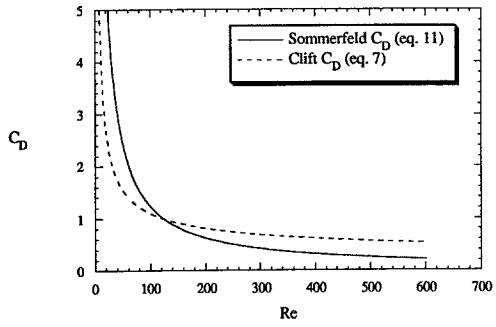

Fig. 2. Sommerfeld and Clift drag coefficients as a function of Reynolds number

density discontinuities. Separate tolerances were required since changes of σ were typically much more severe compared to ρ, thus yielding more relaxed tolerance parameters for σ.

2.3. Interphase coupling

Based on the approximations mentioned in Sect. 1.2, the particles affect the gas through the interphase coupling terms D_i and Q. The drag force per unit volume, D_i, is:

$$D_i = \frac{\pi}{8} n \rho C_D |u_i - u_{pi}| (u_i - u_{pi}) d^2 \tag{6}$$

where summation is not carried out over the indices, d is the particle diameter, and C_D is the coefficient of drag.

Two different C_D's were investigated in the present study. The first C_D is given by Clift et al. (1978) which is based on several sets of steady flow experiments of sphere drag:

$$C_D = \frac{24}{Re}\left(1 + 0.15 Re^{0.687}\right) \tag{7}$$

which is valid for $Re < 800$, where Re is the flow Reynolds number based on slip velocity defined by:

$$Re = \frac{\rho |u_i - u_{pi}| d}{\mu} \tag{8}$$

and where μ is the coefficient of viscosity. For air, Sommerfeld (1985) describes μ as:

$$\mu = \frac{1.458 \times 10^{-5} T^{1.5}}{110 + T} \quad \frac{\text{g}}{\text{cm} \cdot \text{s}} \tag{9}$$

and T is the gas temperature in degrees Kelvin. Olim et al. (1987) noted the following formula for the viscosity of oxygen in referring to their numerical method:

$$\mu = 5.1 \times 10^{-6} T^{0.6487} \quad \frac{\text{g}}{\text{cm} \cdot \text{s}} \tag{10}$$

Sommerfeld (1985) stated that the standard C_D (Eq. (7)) is valid only for steady flows and empirically determined a C_D for unsteady flows based on the experimental two phase shock tube results:

$$C_D = 112 Re^{-0.98} \tag{11}$$

This C_D was derived from laser-Doppler-velocimetry measurements of particle velocities and presumably valid for $\eta < 2.0$ and $1 < M_s < 1.7$.

A comparison of the standard and 'unsteady' C_D's is given in Fig. 2, which shows that for Re numbers above 130, the unsteady C_D will yield much less drag than the standard C_D. There are several other studies of 'unsteady drag coefficients' based on experiments (see Sommerfeld 1985). Recent theoretical work on the unsteady effect on particles has been carried out to include the Basset history term by Mei (1990), for which it was shown that frequency-based unsteady drag was always higher than steady drag for particle Reynolds numbers at least up to 140. It should be noted that for the current study, compressibility effects in the drag were considered to be negligible since slip Mach numbers were small – this was supported by empirical relationships for compressibility (Sommerfeld 1989). However, Olim et al. (1987) retained these terms in their calculations.

The heat transferred from the gas to the particles is described by (Olim et al. 1987):

$$Q = An\left[h(T - \theta) + \sigma^*\left(T^4 - \theta^4\right)\right] \tag{12}$$

where A is the area of the particle (πd^2), h is the coefficient of heat convection, σ^* is the Stefan-Boltzmann constant for radiation, and θ is the particle temperature. The radiation term was ignored, since this contribution was found to be negligible for the present study. The coefficient of heat convection is:

$$h = \frac{Nuk}{d} \tag{13}$$

where Nu is the Nusselt number and the thermal conductivity of the gas, k, is taken as a constant, 1.787×10^3 g/cm·s. Two different Nu numbers were examined; one with:

$$Nu = 2 \tag{14}$$

and a second more robust expression, as:

$$Nu = 2 + 0.459 Pr^{0.333} Re^{0.55} \tag{15}$$

where the Prandtl number, Pr, is taken as a constant, 0.75.

3. Discussion

Since two-dimensional experimental results were not available, only one-dimensional dusty shock attenuations could

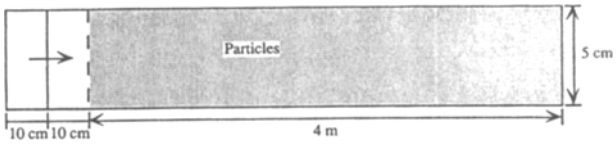

Fig. 3. Initial computational domain

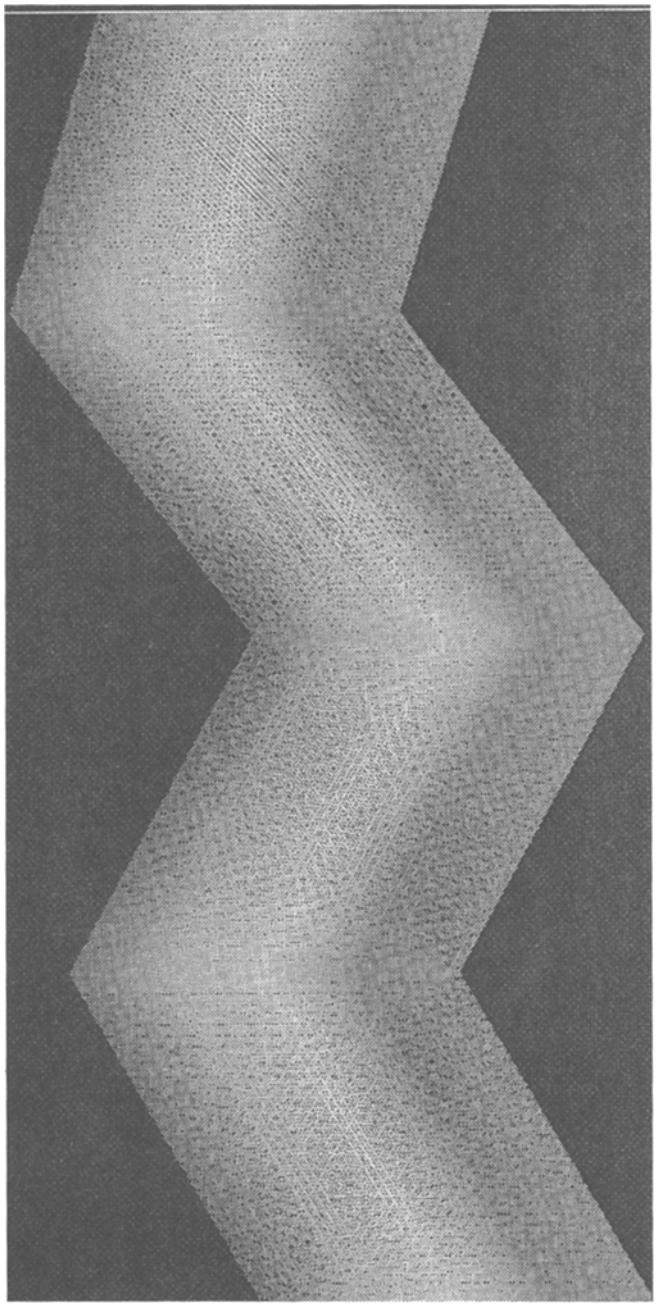

Fig. 4. Particle spatial density before initial refinement

be used to evaluate the performance of the present methodology. However, a two-dimensional formulation and domain was employed. Figure 3 shows the initial computational domain used for all the simulations. A right moving shock is initially located 100 mm upstream of a quiescent particle

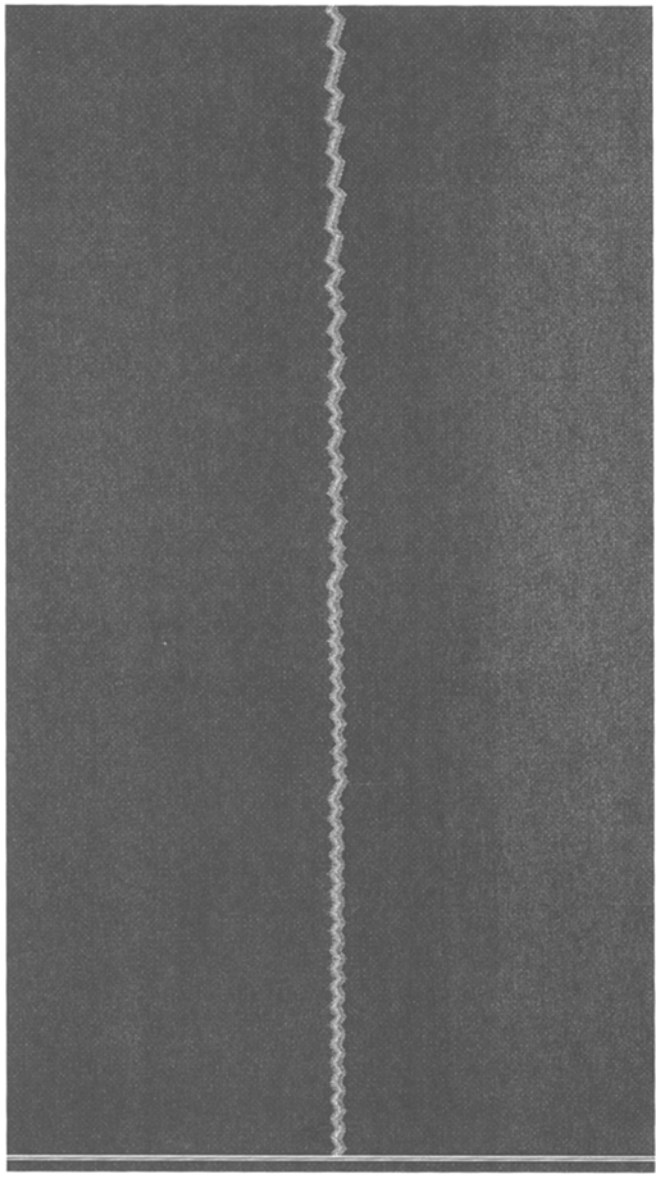

Fig. 5. Particle spatial density after initial refinement

region. Before the time integration is initiated, the initial particle front discontinuity and the shock wave were refined to four levels of refinement from a background mesh, where each refinement level corresponds to a subdivision of one triangular element into four elements. A close-up of the particle discontinuity is shown before (Fig. 4) and after (Fig. 5) this original refinement based on spatial density is completed, and is similar to the refinement across the shock based on gas density before the time integration proceeds.

The mesh dynamic refinement and coarsening for the moving gas and particle discontinuity are shown for a timestep after the shock has entered the particle laden region in Fig. 6, where the shock front is to the right and the particle front is to the left. The minimum element size has a length scale of approximately 0.6 mm. At a later time, Fig. 7 shows gas density (ρ) contours of a typical right-running shock propagating into a dusty gas, using the present numerical method. The reduction in gas density due to particle drag is evident in the gradient which spans the

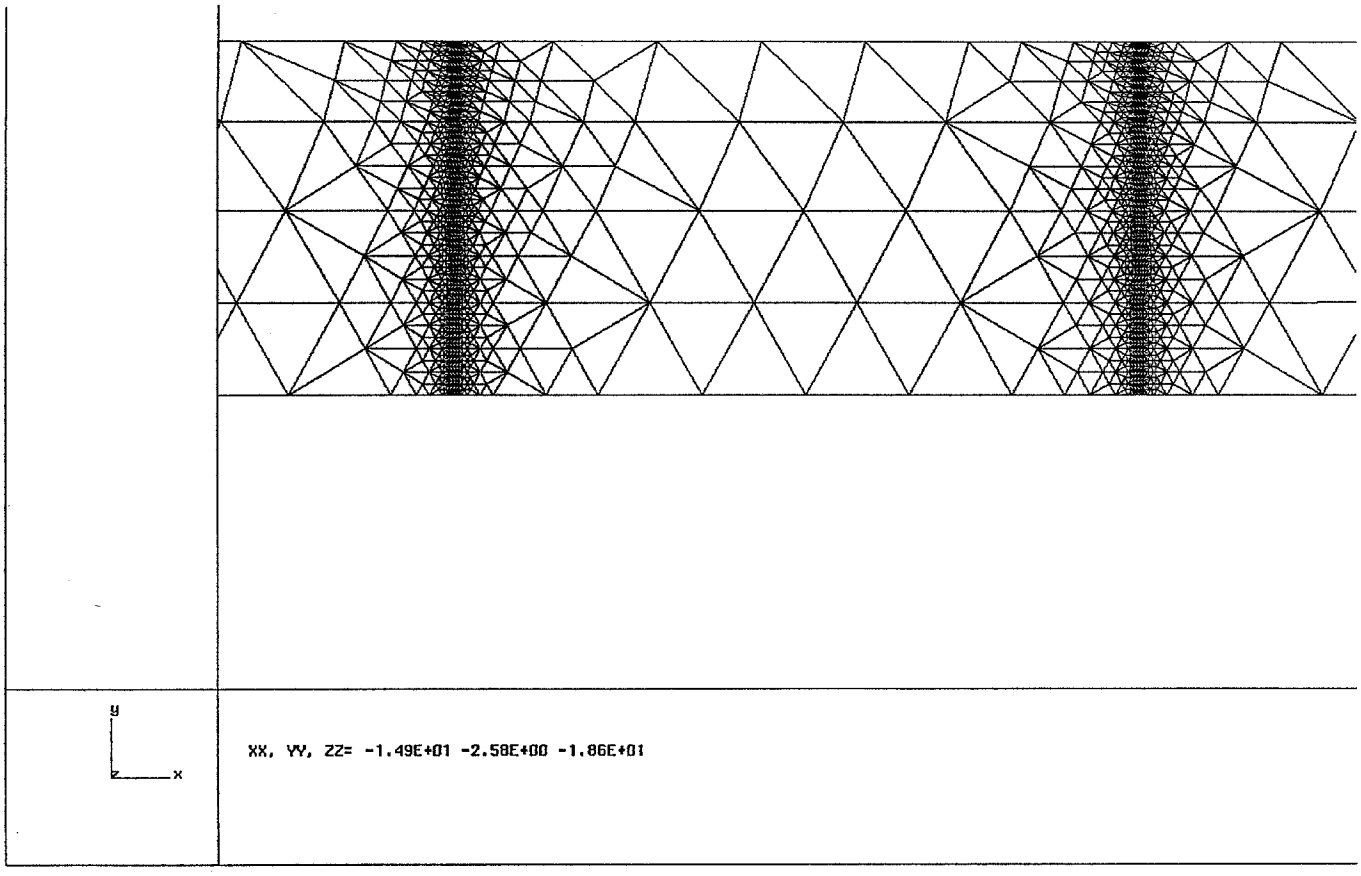

Fig. 6. Mesh refinement and coarsening to shock and particle fronts

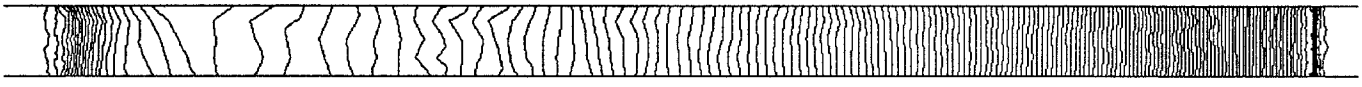

Fig. 7. Gas density contours showing edge of particle laden region on far left, shock discontinuity at the far right, and gradual decrease in gas density left to right indicating shock attenuation

particle laden region behind the shock front and terminates at the far left side where the particle interface is located. Figure 8 shows a close-up of the same gas density contours near the shock overlapped by the mesh, indicating such density discontinuities are typically resolved across four computational cells, similar to that found for the particle density. In general, noise levels are quite low, typically limited to one contour out of 256 equal contours. However, attempts to apply Lapidus diffusion (Löhner et al. 1987) to the calculations in order to further reduce this noise level resulted in numerical instabilities. The reason for this is not known and will be the subject of subsequent research.

Figure 9 shows the Mach number variation due to attenuation of a shock wave propagating into a two-phase flow consisting of air and glass spheres with a diameter of 27 μm (as used in the experiments of Sommerfeld, 1985). The shock is initially at $M_0 = 1.49$ and the loading ratio (η) is 0.63. Results from the present two-phase Eulerian implementation of FEM-FCT are presented along with experimental and numerical results from Sommerfeld. As the shock wave continues to travel through the particle laden region, the exponential type decay of its strength can be seen. In view of the data scatter, all predictions show reasonable agreement with the experimental results. The predictions of Sommerfeld and FEM-FCT with the same 'unsteady' drag coefficient of (11) are quite similar. However, the predictions with the standard drag coefficient exhibit increased attenuation initially, where slip velocities and thus Reynolds numbers are expected to be higher. Such a trend is consistent with the differences noted in Fig. 2.

Figure 10 shows a similar but less rapid attenuation behavior for the same particle loading of 0.63 but a lower M_0 of 1.25. All the predictions agree with the trend of the experimental data, but tend to overestimate the rate of attenuation. The effect of the Nusselt number description shows less attenuation for the simpler and less accurate $Nu = 2$ case for FEM-FCT, which is consistent with the reduction of heat transfer associated with this approximation. The Sommerfeld simulation exhibits an even lower shock strength at four meters as compared to FEM-FCT, whereas predictions of Olim et al. (1987) are closer to the data. It should be noted that Olim et al. employed a viscosity coefficient for oxygen (Eq. (10)) in their calculations; the reason for not using a viscosity for air was not given. Tests with FEM-FCT

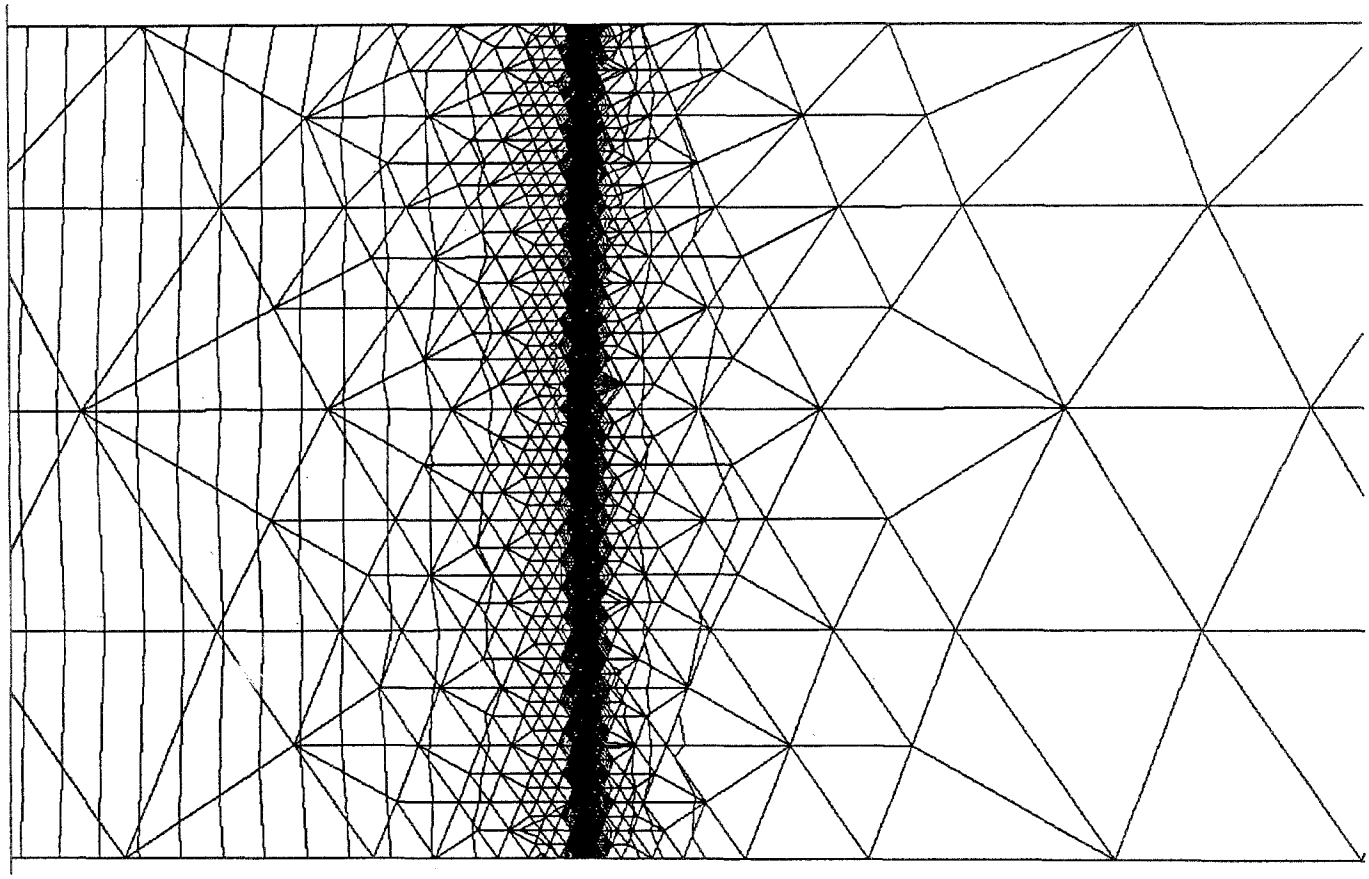

Fig. 8. Close-up of gas density contours across shock superimposed over the mesh

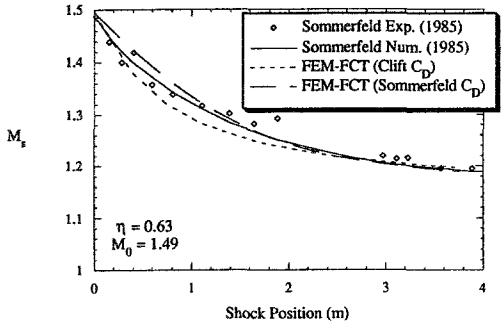

Fig. 9. Shock position vs. M_s for $M_0 = 1.49$, $\eta = 0.63$

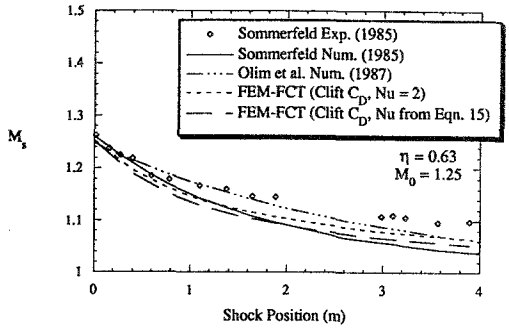

Fig. 10. Shock position vs. M_s for $M_0 = 1.25$, $\eta = 0.63$

showed that substituting the viscosity coefficient given by Olim et al. did not result in any significant change in the flowfield. Since the experimental configuration injected the particle-gas mixture upstream of the shock at a slow upward velocity of 1–3 m/s, numerical tests were also conducted with an initial velocity of 1 m/s of both particles and gas, which showed no significant differences as compared to the quiescent cases.

Figure 11 shows results for an M_0 of 1.48 and an increased η of 1.25, yielding much stronger attenuation as compared to η of 0.63 (Fig. 9). Agreement for the FEM-FCT predictions with experiments is excellent, especially for the first meter of attenuation. The Sommerfeld predictions show reasonable agreement as well but with the same trend of discrepancies noted in Fig. 9, which is presumably a result of the different drag coefficients. A low Mach number shock attenuation case is shown in Fig. 12 for the case of $M_0 = 1.26$ and an η of 0.25. The reduced mass loading led to much less attenuation and the FEM-FCT calculations yielded excellent agreement with the experimental results.

To investigate the slip velocity distribution, the gas and particle velocities a long the lower wall of the tube throughout the shock attenuation region are shown in Fig. 13 at a single time instant of the case with $M_0 = 1.48$ and $\eta = 1.25$ (ca. Fig. 11). From the quiescent unshocked region to the right, the gas velocity discontinuously rises across the shock and then continues to rise through the particle-laden region until it finally reaches its unattenuated value upstream of this region. The particles are continuously accelerated to this same speed, resulting in a maximum slip velocity up-

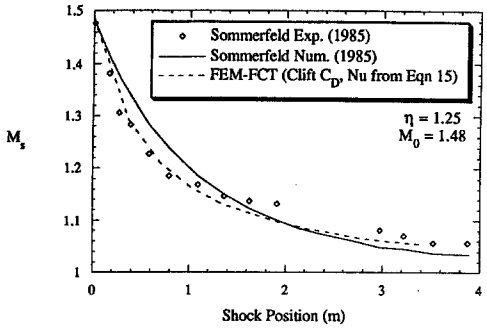

Fig. 11. Shock position vs. M_s for $M_0 = 1.48$, $\eta = 1.25$

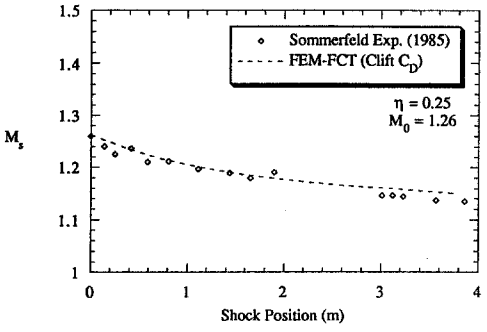

Fig. 12. Shock position vs. M_s for $M_0 = 1.26$, $\eta = 0.25$

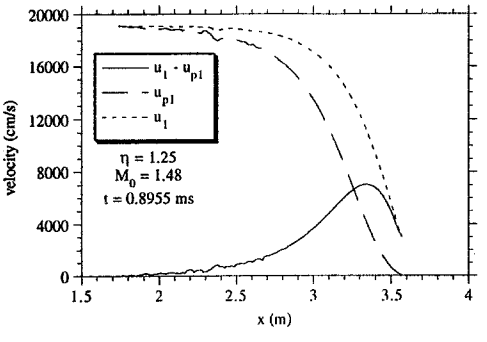

Fig. 13. Velocity distribution due to shock attenuation for $M_0 = 1.48$, $\eta = 1.25$

stream of the shock itself. Some oscillations can be seen near the particle interface region, which may be a result of the absence of Lapidus diffusion in the scheme and will be studied in the future.

Figure 14 shows the distribution of slip Reynolds number through the shock attenuation structure at selected timesteps for the same case. The Reynolds number distribution extends from just downstream of the shock (the rightmost point of each curve) to the end of the two-phase region (the leftmost point of each curve) and are well within the range of the Clift drag coefficient applicability. The distribution shows that the maximum Re typically does not occur immediately behind the shock, rather it is delayed some distance by the relaxation time of the particles. Note, as the shock just enters the particle-laden region, the maximum slip Reynolds number occurs at the shock (e.g. $t = 0.995$ ms); however, as the shock wave is attenuated, the post-shock gas velocity rise

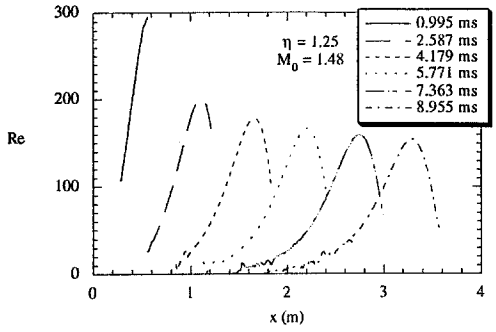

Fig. 14. Reynolds number distribution through the shock attenuation structure at selected timesteps for $M_0 = 1.48$, $\eta = 1.25$

is responsible for the maximum Reynolds number condition. Eventually, when the shock front has been attenuated to a nearly sonic value, the slip Reynolds number distribution should become completely continuous since it will only be caused by the continuous gas velocity rise. Thus it is felt that if an unsteady drag coefficient is to be used, it should probably only be employed at the shock front, which is responsible for only a fraction of the particle acceleration.

In general, the approach of the present study yielded shock wave attenuations near that given by the experimental data. The Sommerfeld (1985) calculations employed an empirical 'unsteady' drag coefficient based on their own experiments. It is not clear whether such an approach is superior. The actual acceleration of the particle due to the time varying slip velocity, expressed as the Basset history term, requires long time evolution of the particle flowfield, which is not practical to store and evaluate in a high resolution multi-dimensional calculation. Based on the analysis of Maxey and Riley (1983), estimates of the order of contribution of the unsteadiness away from the shock front for the present conditions are about three percent of the viscous drag contribution. The authors feel that the standard steady drag coefficient would lead to more robust solutions for complicated flow structures, since it is not based on any specific conditions of flow acceleration. The robustness of the scheme given by Olim et al. (1987) which also used a steady drag coefficient is not easily determined since only a single case was compared directly with experiment in their study.

The overestimation of shock attenuation noted in Fig. 10 for all of the above numerical approaches is interesting. Most of the physical mechanisms that were not taken into account by the computational assumptions would lead to *additional* attenuation as compared to the ideal case. These effects include non-sphericity of the particles (although Sommerfeld's micrographs did not record such deviations); a distribution of diameters as opposed to a single constant diameter (although this was shown to increase drag by less than 1 % based on a simple analysis, using the size distribution given by Sommerfeld); unsteadiness, which typically augments viscous drag (although expected to be small for low particle Reynolds numbers by Mei, 1990); and shock tube viscous effects (although for large flow Reynolds numbers, this should not significantly affect shock speed). It appears that the only effect, other than experimental uncertainties or

bias, that could cause a decrease in the shock attenuation expected from the ideal case is particle clumping, which would result in a lower drag force per particle. It could be that such clumping, which may have been caused by electro-static effects, is less likely to have been maintained for the stronger initial shocks of $M_0 \approx 1.5$ as opposed to the shocks of $M_0 = 1.25$. The second low Mach number case of Fig. 12 clearly did not lead to excessive attenuation predictions, possibly because the lower mass loading may have lessened the particle agglomeration.

Computations for this study were completed on a CRAY Y-MP and typically took 2 hours and 2.2 MWords of memory to complete one adaptive mesh run with approximately 3500 points. In comparison to similar FEM-FCT single-phase calculations, the two-phase approach took approximately twice as much CPU time and thirty percent more memory. The efficiency of the present methodology should be further realized with complex two-dimensional configurations, where structured mesh approaches will require sizable resources to maintain the same degree of resolution possible in the present approach.

4. Conclusion

Two-phase flow equations have been added to a conservative, monotonic flow solver to allow the study of compressible particle and droplet flows, which are important to two-phase shock flows and propulsion systems. The formulation developed in our study employed an Eulerian treatment for the gas and particle phases, both in conserved quantities. The computations were performed using the finite element method-flux corrected transport (FEM-FCT) scheme for the time integration of both phases. A special flux limiting was employed for the particle equations only in order to provide monotonic particle velocity fields and to increase the scheme's computational stability. Adaptive unstructured methodology based on adapting to high gradients of both the fluid and particle densities to provide high resolution was implemented in conjunction with the conservative shock-capturing scheme. This scheme yielded excellent monotonic shock capturing, confined to typically three or four elements across the shock. The shock attenuation of this scheme was then compared with previous experimental and numerical results and was found to yield robust predictions. Various interphase coupling terms were also considered, which led to significant changes in the flow solution. In general, the standard coefficients for momentum and energy transfer of spherical particles were found to be quite reasonable to describe significant shock attenuation.

Acknowledgement. This research was supported by Science Applications International, Corp. (SAIC) under contract 1-5-26905. Computer time was furnished by the National Center for Supercomputing Applications (NCSA) at the University of Illinois at Urbana-Champaign under contract CBT900010N. The authors would also like to acknowledge the assistance of Jim Bacon and Mathew Biggs, undergraduates at UIUC, for graphical processing.

References

Baum JD, Loth E, Löhner R (1990) Numerical simulation of shock interaction with complex geometry canisters. In: Kim Y (ed) Current topics in shock waves. American Institute of Physics, pp 909–914

Boris JP, Book DL (1976) Flux-corrected transport. III. Minimal-error FCT algorithms. J Comp Phys 20:397

Clift R, Grace JR, Weber ME (1978) Bubbles, drops, and particles. Academic Press

Crowe CT (1982) Review – numerical models for dilute gas-particle flows. J Fluid Eng 104:297

Donea J (1984) A taylor-galerkin method for convective transport problems. Int J Num Meth Eng 20:101

Igra O, Ben-Dor G (1980) Parameters affecting the relaxation zone behind normal shock waves in a dusty gas. Israel Journal of Technology 18:159

Löhner R, Morgan K, Zienkiewicz OC (1984) The solution of non-linear hyperbolic equation systems by the finite element method. Int J Num Meth Fluids 4:1043

Löhner R, Morgan K, Zienkiewicz OC (1985) An adaptive finite element procedure for high speed flows. Computational Methods in Applied Mechanics Engineering 51:441

Löhner R, Morgan K, Peraire J, Vahdati M (1987) Finite element flux corrected transport (FEM-FCT) for the Euler and Navier-Stokes equations. International Journal for Numerical Methods in Fluids 7:1093

Löhner R, Baum JD, Loth E, Ramamurti R (1989) A finite element solver for axisymmetric compressible flows. AIAA-89-1794, AIAA 20th fluid dynamics and plasma dynamics and lasers conference, Buffalo NY, June 12–14.

Loth E, Baum JD, Löhner R (1990a) Formation of shocks within axisymmetric flows. AIAA-90-1655, AIAA 21st fluid dynamics and plasma dynamics and lasers conference, Seattle WA.

Loth E, Kailasanath K, Löhner R (1990b) Supersonic flow over an axisymmetric backward facing step. AIAA-90-1580, AIAA 22nd fluid dynamics and plasma dynamics and lasers conference, Seattle, WA, June.

Maxey MR, Riley JJ (1983) Equation of motion for a small rigid sphere in a non-uniform flow. Phys of Fluids 26:883

Mei R (1990) Particle dispersion in isotropic turbulence and unsteady particle dynamics at finite reynolds number. PhD Dissertation for TAM, University of Illinois at Urbana-Champaign

Olim M, Igra O, Mond M, Ben-Dor G (1987) A general attenuation law of planar shock waves propagating into dusty gases. In: Proceedings of the 16th international symposium on shock waves and shock tubes. pp 217–225

Sommerfeld M (1985) The unsteadiness of shock waves propagating through gas-particle mixtures. Experiments in Fluids 3:197

Sommerfeld M (1989) The influence of solid particles on the structure of supersonic free jet flows. In: Proceedings of the 17th international symposium on shock tubes and waves. pp 745–750

Zalesak ST (1979) Fully multidimensional flux-Corrected transport algorithms for fluids. J Comp Phys 31:335–362

This article was processed using Springer-Verlag TEX Shock Waves macro package 1.0 and the AMS fonts, developed by the American Mathematical Society.